MIT Open Access Articles

Design of a custom vapor transport co-deposition system for scalable production of perovskite solar cells

The MIT Faculty has made this article openly available. ***Please share*** how this access benefits you. Your story matters.

Citation: Ella Wassweiler, Anurag Panda, Tamar Kadosh, Thienan Nguyen, Wan-Ju Hsu, Emma Pettit, Russell J. Holmes, Harry Tuller, Vladimir Bulovic; Design of a custom vapor transport co-deposition system for scalable production of perovskite solar cells. J. Vac. Sci. Technol. A 1 September 2023; 41 (5): 052801.

As Published: 10.1116/6.0002668

Publisher: American Vacuum Society

Persistent URL: https://hdl.handle.net/1721.1/156893

Version: Final published version: final published article, as it appeared in a journal, conference proceedings, or other formally published context

Terms of use: Creative Commons Attribution

Massachusetts Institute of Technology

Journal of Vacuum Science and Technology A

RESEARCH ARTICLE | JULY 12 2023

Design of a custom vapor transport co-deposition system for scalable production of perovskite solar cells

Ella Wassweiler ; Anurag Panda ; Tamar Kadosh ; Thienan Nguyen; Wan-Ju Hsu; Emma Pettit; Russell J. Holmes ; Harry Tuller; Vladimir Bulovic

J. Vac. Sci. Technol. A 41, 052801 (2023)
https://doi.org/10.1116/6.0002668
CHORUS

View Online
Export Citation

18 September 2024 17:55:02

JVST A
Journal of Vacuum Science & Technology A

ARTICLE

pubs.aip.org/avs/jva

Design of a custom vapor transport co-deposition system for scalable production of perovskite solar cells

Cite as: J. Vac. Sci. Technol. A **41**, 052801 (2023); doi: 10.1116/6.0002668
Submitted: 12 March 2023 · Accepted: 12 June 2023 ·
Published Online: 12 July 2023

View Online

Export Citation

CrossMark

Ella Wassweiler,[1,a)] Anurag Panda,[1] Tamar Kadosh,[2] Thienan Nguyen,[1] Wan-Ju Hsu,[3] Emma Pettit,[3] Russell J. Holmes,[3] Harry Tuller,[2] and Vladimir Bulovic[1,b)]

AFFILIATIONS

[1]Department of Electrical and Computer Engineering, MIT, School of Engineering, 50 Vassar St., Cambridge, Massachusetts 02142
[2]Department of Materials Science and Engineering, MIT, School of Engineering, 77 Massachusetts Ave., Cambridge, Massachusetts, 02139
[3]Department of Chemical Engineering and Materials Science, University of Minnesota, 421 Washington Ave. SE, Minneapolis, Minnesota 55455

[a)]**Author to whom correspondence should be addressed:** ella.wassweiler@gmail.com
[b)]**Electronic mail:** bulovic@mit.edu

18 September 2024 17:55:02

ABSTRACT

Vacuum-deposited perovskites provide a more direct path to manufacturing large area solar cells because of ready compatibility with multi-layered architectures and historic use in the electronics industry. However, vacuum compatible co-deposition of organic-inorganic perovskites remains difficult due to issues of precisely controlling the organic precursor flux. Here, we demonstrate a manufacturing prototype specifically designed for co-depositing organic-inorganic perovskites and evaluate it with respect to the influence of process parameters on film growth. Through depositing and characterizing methylammonium lead iodide ($MAPbI_3$) perovskite films, we highlight the necessary design requirements while measuring the influence of film growth parameters on deposition rate and perovskite phases.

© 2023 Author(s). All article content, except where otherwise noted, is licensed under a Creative Commons Attribution (CC BY) license (http://creativecommons.org/licenses/by/4.0/). https://doi.org/10.1116/6.0002668

I. INTRODUCTION

Recent rapid advances in perovskite materials have brought about improvements to a variety of optoelectronic devices[1–3] including solar cells. Specifically, vapor-deposition for solar cells has several advantages stemming from the lack of solvent use, which include increased compatibility with complex architectures, tight control over film composition,[4,5] and familiarity with manufacturing.[6] As a result, recent literature has explored vapor-deposited perovskites both with a number of precursors[7,8] and the techniques available[9–11] and have attained device efficiencies as high as 24.1%.[12] With the increase in deposition types available, researchers have begun to explore vapor-deposition on a larger scale.[13–16]

Both increases in types of deposition techniques available and in deposition scale are brought about by advances in the fundamental understanding of how to control perovskite precursors under vacuum.[17,18] Deposition parameters such as pressure and substrate temperature are found to control grain size,[19] composition,[20,21] defect density,[22] and crystallinity.[23] These advances aid in defining more desirable deposition regimes[24] and overall film growth processes.[25] Co-deposition is becoming the focus of investigation because of the well-mixed nature of precursors during film growth and increase in deposition speed improving compatibility with manufacturing.

However, to date, most advances have been demonstrated utilizing high-vacuum thermal evaporation[13,26,27] that is incompatible with manufacturing due to low film growth rates. Translating advances, including co-deposition film growth, high efficiency solar cells, and increasingly stable solar cells into

manufacturing-compatible techniques, even vapor-based techniques, are not straightforward. One vapor-manufacturing technique, vapor transport deposition (VTD), decouples sublimation temperature from the deposition rate through using a carrier gas.[17,28,29] While this increases the overall deposition rate by orders of magnitude, it also introduces additional variables that are not adequately studied in the literature using thermal evaporation.

To continue to drive the perovskite-field toward manufacturing compatibility, researchers need to consider the deposition techniques they are using and, specifically, how the tools used could be integrated into a manufacturing line. However, most high-performing solar cells contain a mix of organic and inorganic precursors that need to be handled differently under vacuum. Organic precursors, such as methylammonium iodide (MAI), present unique challenges to deposition rate control. Historically, precursors under vacuum are monitored and controlled via a quartz crystal monitor (QCM). However, MAI has largely been resistant toward developing a simple QCM rate. Therefore, in literature, there are two prevalent techniques for depositing the MAI precursor. One advocates for the use of MAI partial pressure during deposition since it is the most reproducible[30–32] The other argues that with proper calibration and understanding that the quartz crystal monitors (QCMs) provide the more accurate assessment.[25]

To handle different styles of precursors, new VTD system designs frequently make use of the bi-directional gas flow[9,24] or two-step processes[33,34] to tightly control these different precursor classes. However, these systems either rely on sequential deposition[28] for inorganic versus organic components or all-inorganic perovskites.[35,36] Therefore, a new variety of vapor co-deposition tools need to be developed that can both be used on a manufacturing line and simultaneously handle unique perovskite precursors.

Here, we demonstrate the custom design of a VTD prototype manufacturing system with a novel material handling capability and compatibility with a wide range of both precursor materials and deposition parameters. We use the model perovskite system methylammonium lead iodide ($MAPbI_3$) to demonstrate the wide material characteristics that are compatible with co-deposition in a VTD system. Finally, we establish a fundamental understanding of a co-deposition VTD film growth that can be used by future system designs and processes.

II. EXPERIMENT

A. Materials and methods

MAI powders were purchased from Luminescence Technology Corporation. PbI_2 powders were from either TCI Chemicals or Alfa Aesar. All precursor powders were stored under nitrogen until loaded into the chamber.

Glass and silicon substrates were cleaned by sonication in acetone (Sigma-Aldrich) followed by sonication in IPA (Sigma-Aldrich), each for 10 min. After each sonication, the substrates are blown dry using nitrogen gas.

All films were deposited on glass using the VTD system and deposition parameters described in the main text. Film thicknesses were measured via AFM or scanning electron microscopy (SEM).

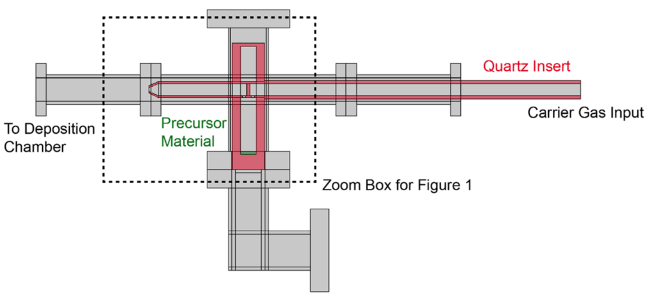

FIG. 1. CAD model of one material arm.

B. Drawings and simulations

Computer Aided Design (CAD) drawings prepared via Solidworks.

Within COMSOL, we used the laminar flow, the heat flow in fluids, and dilute species modules to replicate the material arm as shown below:

C. Characterization techniques

For SEM, the films were measured either with a Zeiss Gemini 450 SEM in MIT.nano or a Zeiss Merlin High-Resolution SEM in MIT Materials Research Laboratory.

The atomic force microscope used was an Asylum Research Cypher VRS AFM in tapping mode at MIT.nano.

X-ray diffraction was performed on a Rigaku Smartlab Multipurpose Diffractometer in the MIT Materials Research Laboratory. The settings were PB-PSA GIXD with 0.02 step size and a rate of 0.6 s/step.

III. RESULTS AND DISCUSSION

Current vacuum deposition systems rely on the use of material boats and shutters to control when deposition occurs. However, the available valves and evaporation boats on the market today do not always meet the needs of VTD chambers (see supplementary material[45]), especially when used with typical perovskite precursors such as metal halides or organic components. Therefore, to be compatible with high temperature sublimation while also tightly controlling the onset of deposition, we needed to create our own design.

As shown in Fig. 1(a), the insert contains two independent segments both made of quartz. The green, inner tube is used for carrier gas injection. Close to the end of the quartz tube is a wall that directs the carrier gas flow into the selected chamber and back into the green, carrier tube before entering the deposition chamber. The black, outer sections are separated into two different small chambers. The top chamber is covered with a quartz cap and is used as a material bypass. The lower chamber is a material reservoir that contains the precursor power heated to sublimation temperature.

In the Off position, the quartz insert closes by rotating the openings on the green, carrier gas injection tube to pass through the bypass chamber. When the valve is turned to the On position,

18 September 2024 17:55:02

© Author(s) 2023

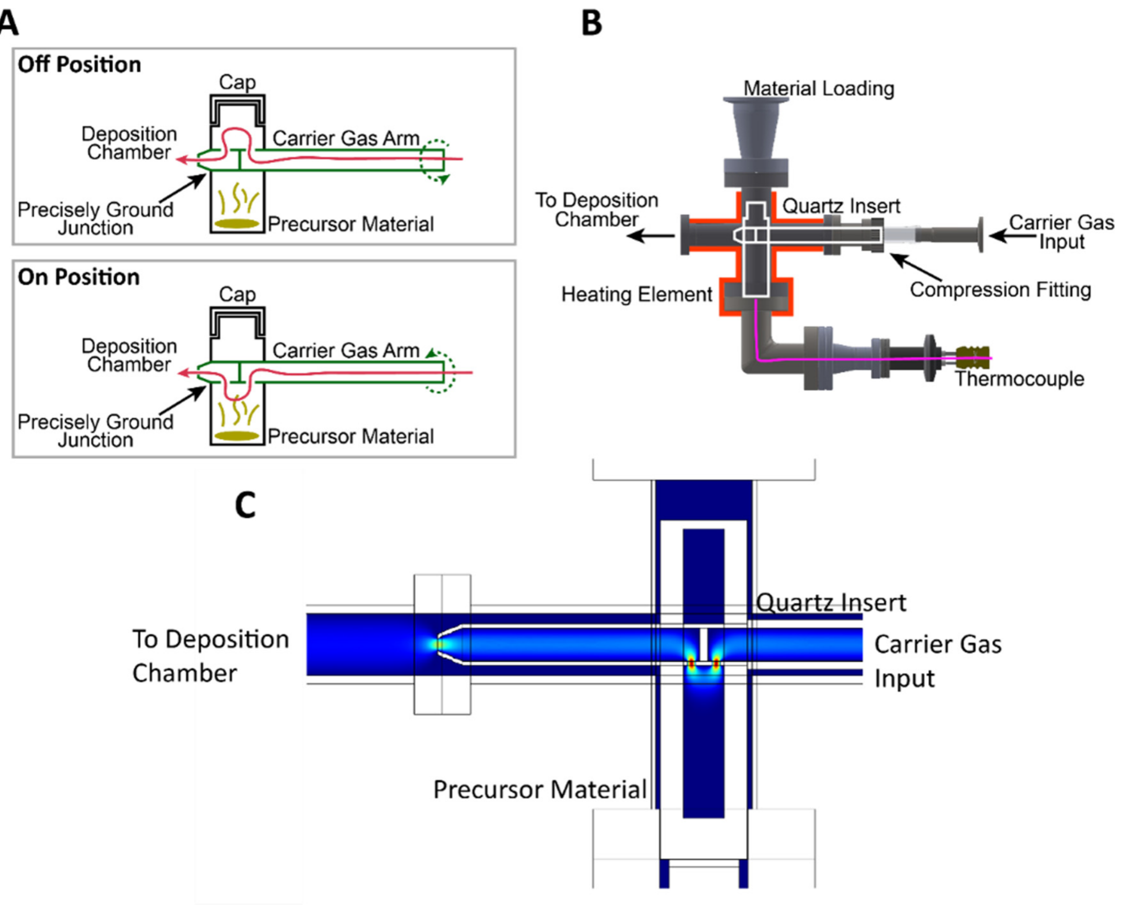

FIG. 2. Quartz insert design and fluid flow simulation. (a) Functional diagram of the inner portion, made of quartz, showing the precursor location and fluid flow in On and Off Positions. (b) CAD drawing of the quartz insert inside the larger deposition chamber. (c) COMSOL simulation of the fluid flow throughout the entire quartz insert and material arm.

18 September 2024 17:55:02

the holes face the precursor material reservoir and a carrier gas is allowed to flow through the sublimed vapors and out into the deposition chamber. During use, the quartz insert is placed into a stainless-steel vacuum chamber as shown in Fig. 1(b) to become compatible with the stainless-steel-dominated vacuum equipment.

To further investigate the material holder's capabilities, we designed a simulation using the finite elemental analysis software COMSOL. Since we designed the system to operate using the carrier gas as the primary determinant of deposition rate, we assume operation in the laminar flow regime and with a dilute amount of precursor material.

As seen in Fig. 1(c), the velocity profile out of the quartz insert nozzle rapidly reaches a continuous, stable flow. Additionally, the carrier gas interacts with only the very top volume of the reservoir containing the precursor material. This is significant because it means that the carrier gas is only flowing through the top volume of the saturated precursor vapors, making it more likely that a saturation of partial precursor pressure will be maintained throughout deposition. Therefore, the carrier gas flow rate, not evaporation rate, determines the material flux out of the quartz insert.

Through careful wrapping of the material arm stainless-steel chamber with heating tape and thermocouples, we maintain consistent temperature throughout (see supplementary material[45]). High concentrations of precursor materials are successfully contained to within the quartz section of the material arm, which minimizes any potential degradation due to the reactive iodine subcomponent. With this quartz insert design as the basis for the design of the full VTD system, we set up two different material arms to co-deposit $MAPbI_3$.

Figure 2(a) is a diagram of the full VTD system. By using individual precursor material arms, the system can tailor deposition parameters to be specific to that material. Only after the initial start of material transport does it start to interact with the other precursor. Decoupling the precursor deposition parameters allows for co-deposition while minimizing degradation mechanisms associated with sublimation temperature.[37,38]

© Author(s) 2023

The material arm and deposition chamber geometry allow for continuous heating from the input of the carrier gas until slightly past the substrate. The wrapping style and amount of heater tape is tailored to both the geometry and thermal mass of each chamber section with thermocouples checking for temperature variation (see supplementary material[45] for more information). The substrate is moved via a stage from the loading chamber and into the deposition chamber (indicated by the dotted arrow). A moving stage allows for gas and material flow to be maintained despite substrate changes. There are individual backing lines to a dry roughing pump for both deposition and loading chambers. Therefore, both can be pumped down independently. Only the line from the loading chamber is used during deposition to maintain a uniform flux across the substrate. With this system, we can achieve base pressures of low 10^{-2} Torr and deposition pressures of commonly 7×10^{-2} Torr.

With this new VTD manufacturing prototype design, we began to investigate co-deposition of $MAPbI_3$ perovskite. Each precursor has its own unique set of challenges and its own unique role in the deposition process. Therefore, understanding the unique challenges and roles associated with each precursor is a necessary prerequisite to their co-deposition.

In Figs. 3(a) and 3(b), we focus on the deposition of MAI only on bare silicon substrates. In Fig. 3(a), we observe a trend downward in film thickness with an increase in sublimation temperature, even with substrate temperature kept constant. This could be indicative of an increase in degradation even with a 20 °C change in sublimation temperature. As the MAI precursor material degrades, it can preferentially form gaseous byproducts such as methylamine gas, iodomethane, hydroiodic acid, and ammonia.[38,39] These byproducts would not deposit on the substrate and thereby cause an overall thinner film. However, within each of these sublimation temperatures, there is a mild trend similar to the equilibrium/kinetic regime theory used in organic vapor phase deposition.[41] Therefore, an increase in the carrier gas flow rate causes an increase in the deposition rate only to a certain extent. After a certain carrier gas flow rate, the deposition rate is determined by the sublimation rate, which for MAI can be difficult to determine. Based on this graph, the lowest sublimation temperature should be used with a carrier gas flow rate below about 11 SCCM in order to obtain both the highest deposition rate possible and control deposition via the carrier gas. Additionally, as seen in Fig. 3(b), the increase in the carrier flow rate changes both the deposition rate and the resultant morphology. Smaller grains are seen with the higher deposition flux, which may also assist in conversion to perovskite during co-deposition.

Each of the PbI_2 films in Fig. 3(c) is grown with different deposition parameters and then measured via x-ray diffraction (XRD). Interestingly, not all deposition parameters give the same phases. Each film shows the characteristic peak at 12.7° but to different extents. In the middle XRD graph, the peak at 25.4° dominates compared to the peak at 12.7°. Additionally, at the higher sublimation temperatures and carrier gas flow rates, there is an increase in the amorphous phase from around 22° to 33°. Only at 20 SCCM and with 325 °C sublimation rate, the XRD graph shows a clear peak at 12.7° and no other features. When translating these deposition parameters and resulting deposition rates to the co-deposition process, it is important to watch whether these phases translate into the perovskite film. Normally less dominant peaks may significantly contribute to perovskite phases seen by films deposited by VTD. When moving to co-deposition of $MAPbI_3$ films (see supplementary material[45]), the 220 phase is found to dominate. While contribution from the 110 phase is still significant, the increased presence of the 220 phase may indicate the higher 2Theta contributions from underlying PbI_2 formation from fast deposition translates into the final perovskite films.

With these understandings of the behavior of perovskite precursors, we investigate another parameter deeply influential to the manufacturing process, deposition rate. Figure 4 displays different process parameters that influence the deposition rate.

We examined the influence of chamber pressure on film formation. Similar to low pressure chemical vapor deposition, we found that chamber pressure has a reciprocal relation to the deposition rate; thus, lower thickness was obtained under a higher pressure, for a fixed deposition time of 30 min (Fig. 5). This effect was also demonstrated in our previous sequentially deposited VTD

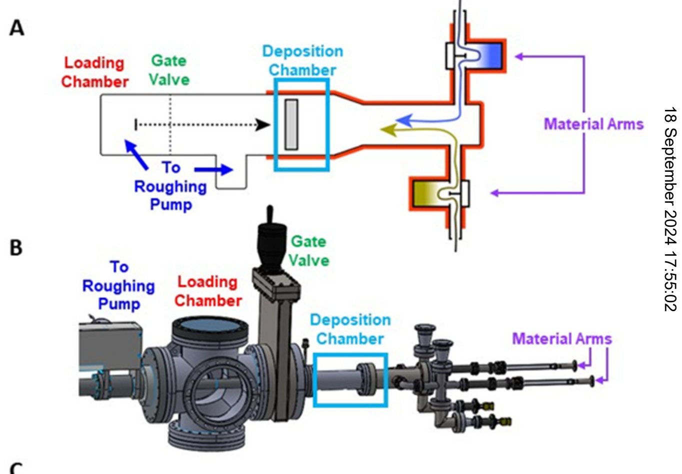

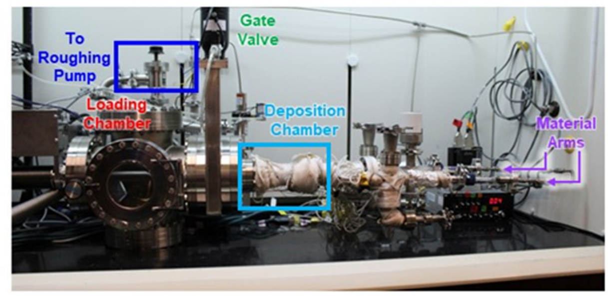

FIG. 3. Design of the full VTD system. (a) Diagram of significant locations within the chamber, including, loading chamber, gate valve, deposition chamber, lines to roughing pump, and material arms. (b) CAD of the Constructed System. (c) Image of the constructed system highlighting the same significant locations as in the above diagram.

18 September 2024 17:55:02

© Author(s) 2023

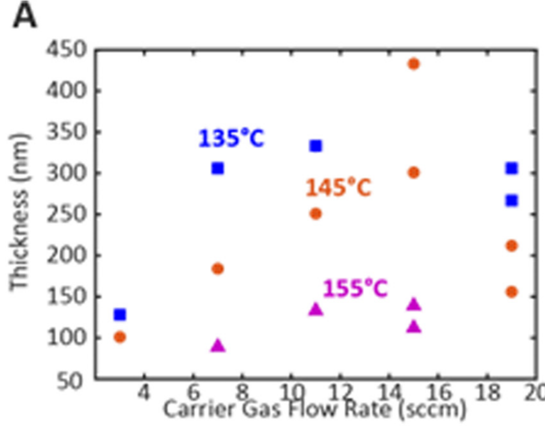

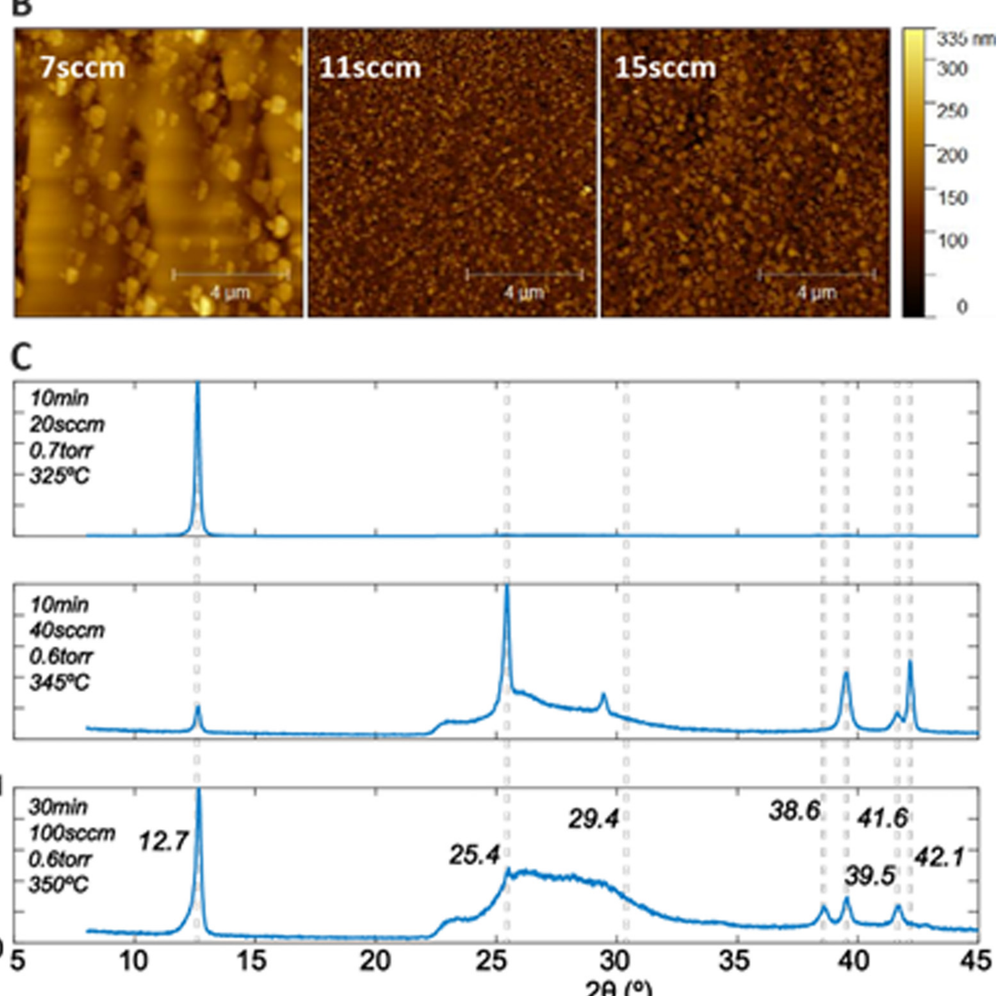

FIG. 4. Deposition of individual precursors on silicon substrates. (a) MAI film thickness vs. carrier gas flow rate vs. sublimation temperature after a 10 min deposition and at 0.7 Torr. (b) Atomic force microscopy images of MAI films at 145 °C sublimation temperature and differing carrier gas flow rates also after a 10 min deposition and at 0.7 Torr. (c) X-ray diffraction graphs of PbI_2 films deposited via different processing conditions. All films are thicker than 100 nm.

18 September 2024 17:55:02

© Author(s) 2023

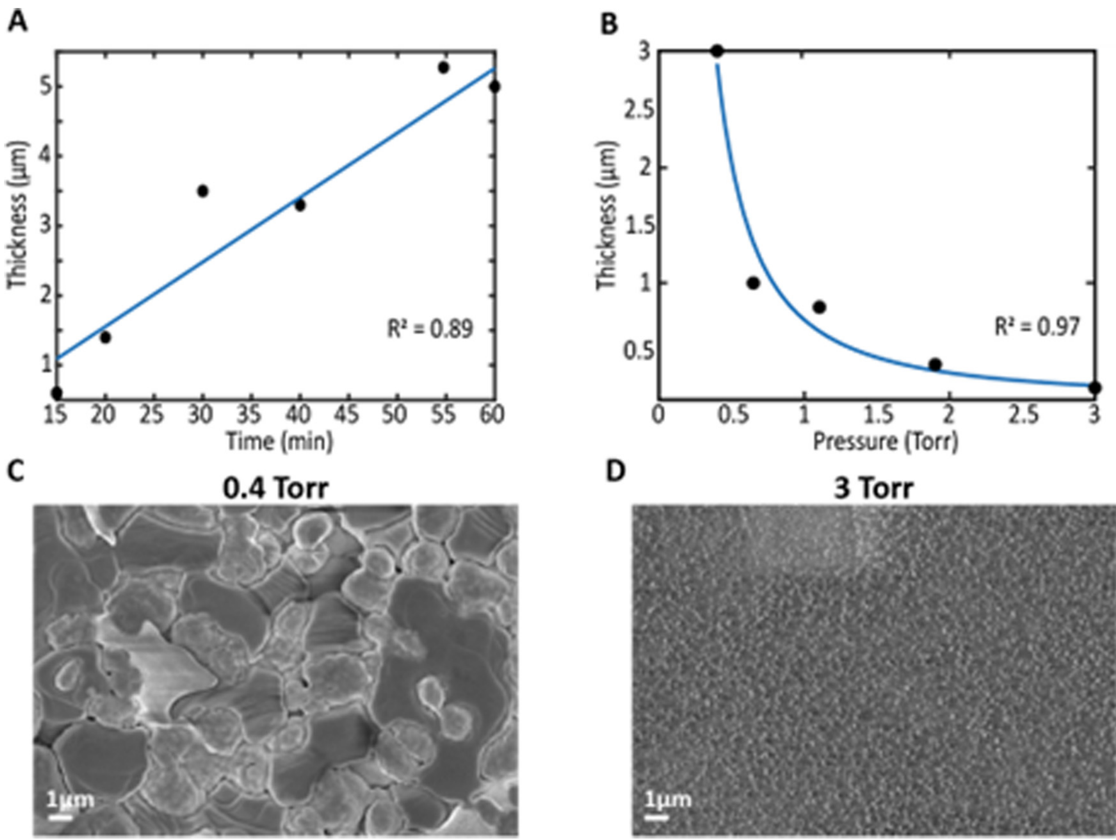

FIG. 5. Co-deposited $MAPbI_3$ perovskite films on glass. (a) Film thickness vs. deposition time with a linear fit. Deposition parameters include: 350 °C sublimation temperature for PbI_2, 175 °C deposition temperature for MAI, 10 SCCM PbI_2 carrier gas flow rate, 3 SCCM MAI carrier gas flow rate. (b) Thickness vs. deposition pressure with a deposition time of 30 min. The thickness follows an exponential curve. The other deposition parameters include the following: 350 °C sublimation temperature for PbI_2, 175 °C deposition temperature for MAI, 10 SCCM PbI_2 carrier gas flow rate, and 3 SCCM MAI carrier gas flow rate. (c) Perovskite film morphology with a deposition pressure of 0.4 Torr and thickness around 3 μm. Film from (b). (d) Perovskite film morphology with a deposition pressure of 3 Torr and thickness around 100 nm. Film from (b).

18 September 2024 17:55:02

system.[28] It is important to note, during the co-deposition process, that the MAI precursor may behave differently than deposited alone. The changes to sticking coefficients[25] with the presence of PbI_2 and $MAPbI_3$ as well as the changes to degradation product interactions with the substrate[41,42] suggest that the deposition rate will be dependent on other materials forming the film. A potential explanation for this observation is related to the kinetic theory of gases: under low pressures, gas molecules have a lower tendency for collisions, and their mean free path is higher, which allows more time for acceleration, increasing their velocity. Hence, gas molecules under lower pressures reach the substrate faster to form a thicker film in a shorter time.[43] Grain size is shown to have a weaker dependence on chamber pressure. However, at the highest pressure tested, domains were in the sub-micrometer scale. Previous studies on organic perovskites have demonstrated that domain growth is equi-axial[44] and, therefore, can be limited by film thickness. Sub-micrometer domains are, therefore, expected for the ~100 nm film formed under a chamber pressure of 3 Torr.

Under co-deposition processes, the film thickness is linearly dependent on the deposition time. Therefore, when using a VTD process, the vacuum systems can use simplified control electronics when paired with our custom quartz insert in material arm design. Even with the MAI sticking coefficient dependent on a wide range of deposition parameters, tight control over this organic precursor can be maintained.

IV. CONCLUSIONS

In conclusion, we systematically describe a VTD manufacturing prototype, which demonstrates a novel method for tailoring control of both organic and inorganic precursors. Furthermore, we use the system to analyze important process parameters to determine research directions to move vacuum-processed perovskites closer to manufacturing. With this added understanding of manufacturing-related deposition processes, we hope to empower investigation enabling perovskite solar cells to be manufactured at scale.

© Author(s) 2023

ACKNOWLEDGMENTS

This material was based upon work supported by the U.S. Department of Energy's Office of Energy Efficiency and Renewable Energy (EERE) under the Solar Energy Technologies Office Award No. DE-EE0009514. The views expressed herein do not necessarily represent the views of the U.S. Department of Energy or the United States Government. Funding was also received from the MIT-TATA GridEdge program.

AUTHOR DECLARATIONS

Conflict of Interest

Portions of the paper have previously been published in Ella Wassweiler's Ph.D. thesis entitled "Vapor Transport Deposition for Perovskite Solar Cells." Thesis copywrite available upon request. Additionally, portions have also been submitted as a U.S. patent application.

Author Contributions

Ella Wassweiler: Conceptualization (equal); Data curation (equal); Formal analysis (equal); Investigation (equal); Methodology (equal); Project administration (equal); Supervision (equal); Writing – original draft (equal); Writing – review & editing (equal). **Anurag Panda:** Conceptualization (equal); Methodology (equal); Project administration (equal). **Tamar Kadosh:** Data curation (supporting); Investigation (supporting); Methodology (supporting). **Thienan Nguyen:** Investigation (supporting). **Wan-Ju Hsu:** Conceptualization (supporting); Formal analysis (supporting). **Emma Pettit:** Conceptualization (supporting); Formal analysis (supporting). **Russell J. Holmes:** Conceptualization (supporting); Formal analysis (supporting). **Harry Tuller:** Conceptualization (supporting); Formal analysis (supporting). **Vladimir Bulovic:** Conceptualization (equal); Formal analysis (equal).

DATA AVAILABILITY

The data that support the findings of this study are available from the corresponding author upon reasonable request.

REFERENCES

[1] R. Zhao, Z. Gu, P. Li, Y. Zhang, and Y. Song, Adv. Mater. Technol. **7**, 2101124 (2022).
[2] X. Xu, Y. Wang, H. Meng, T. Zhu, D. Yan, W. Zhu, S. Liu, and Q. Zhao, Matter **5**, 2086 (2022).
[3] J. Gong, M. Flatken, A. Abate, J. P. Correa-Baena, I. Mora-Seró, M. Saliba, and Y. Zhou, ACS Energy Lett. **4**, 861 (2019).
[4] J. Ávila, C. Momblona, P. P. Boix, M. Sessolo, and H. J. Bolink, Joule **1**, 431 (2017).
[5] M. Shtein, *Organic Vapor Phase Deposition and Vapor Jet Printing for Electronic and Optoelectronic Device Applications* (Princeton University, Princeton, New Jersey, 2004).
[6] R. C. Powell, "Research Leading to High-Throughput Manufacturing of Thin-Film CdTe PV Modules: Annual Subcontract Report, September 2004–September 2005" (2004).
[7] L. Gil-Escrig, C. Momblona, M. G. La-Placa, P. P. Boix, M. Sessolo, and H. J. Bolink, Adv. Energy Mater. **8**, 1703506 (2018).
[8] M. Kam, Y. Zhu, D. Zhang, L. Gu, J. Chen, and Z. Fan, Solar RRL **3** (2019).
[9] S. Ngqoloda, C. J. Arendse, T. F. Muller, P. F. Miceli, S. Guha, L. Mostert, and C. J. Oliphant, ACS Appl. Energy Mater. **3**, 2350 (2020).
[10] G. Kim, S. An, S. K. Hyeong, S. K. Lee, M. Kim, and N. Shin, Chem. Mater. **31**, 8212 (2019).
[11] A. J. Harding, A. G. Kuba, B. E. McCandless, U. K. Das, K. D. Dobson, B. A. Ogunnaike, and W. N. Shafarman, RSC Adv. **10**, 16125 (2020).
[12] S. Wang *et al.*, Joule **6**, 1344 (2022).
[13] J. Li *et al.*, Joule **4**, 1035 (2020).
[14] S. R. Ratnasingham, L. Mohan, M. Daboczi, T. Degousé, R. Binions, O. Fenwick, J.-S. Kim, M. A. Mclachlan, and J. Briscoe, Mater. Adv. **2**, 1606 (2021).
[15] M. Wang and C. J. Carmalt, ACS Appl. Energy Mater. **5**, 5434–5448 (2021).
[16] T. Abzieher, IEEE J. Photovolt. **9**, 1249 (2019).
[17] C. P. Clark, B. Voigt, E. S. Aydil, and R. J. Holmes, Sustain. Energy Fuels **3**, 2447 (2019).
[18] Q. Guesnay, F. Sahli, C. Ballif, and Q. Jeangros, APL Mater. **9**, 100703 (2021).
[19] K. B. Lohmann, J. B. Patel, M. U. Rothmann, C. Q. Xia, R. D. J. Oliver, L. M. Herz, H. J. Snaith, and M. B. Johnston, ACS Energy Lett. **5**, 710 (2020).
[20] M. Roß, L. Gil-Escrig, A. Al-Ashouri, P. Tockhorn, M. Jošt, B. Rech, and S. Albrecht, ACS Appl. Mater. Interfaces **12**, 39261 (2020).
[21] T. Gallet, R. G. Poeira, E. M. Lanzoni, T. Abzieher, U. W. Paetzold, and A. Redinger, ACS Appl. Mater. Interfaces **13**, 2642 (2021).
[22] A. Ng *et al.*, ACS Appl. Mater. Interfaces **8**, 32805 (2016).
[23] C. Wittich, E. Mankel, O. Clemens, K. Lakus-Wollny, T. Mayer, W. Jaegermann, and H. J. Kleebe, Thin Solid Films **650**, 51 (2018).
[24] T. Moser, K. Artuk, Y. Jiang, T. Feurer, E. Gilshtein, A. N. Tiwari, and F. Fu, J. Mater. Chem. A **8**, 21973 (2020).
[25] B. S. Kim, L. Gil-Escrig, M. Sessolo, and H. J. Bolink, J. Phys. Chem. Lett. **11**, 6852 (2020).
[26] M. Sessolo, C. Momblona, L. Gil-Escrig, and H. J. Bolink, MRS Bull. **40**, 660 (2015).
[27] I. Susic, L. Gil-Escrig, F. Palazon, M. Sessolo, and H. J. Bolink, ACS Energy Lett. **14**, 13 (2022).
[28] M. T. Hoerantner *et al.*, ACS Appl. Mater. Interfaces **11**, 32928 (2019).
[29] C. P. Clark, J. E. Mann, J. S. Bangsund, W. J. Hsu, E. S. Aydil, and R. J. Holmes, ACS Energy Lett. **5**, 3443 (2020).
[30] T. Abzieher *et al.*, Adv. Funct. Mater. **31**, 2104482 (2021).
[31] K. L. Heinze, O. Dolynchuk, T. Burwig, J. Vaghani, R. Scheer, and P. Pistor, Sci. Rep. **11**, 15299 (123AD).
[32] V. Arivazhagan, J. Xie, Z. Yang, P. Hang, M. M. Parvathi, K. Xiao, C. Cui, D. Yang, and X. Yu, Sol. Energy **181**, 339 (2019).
[33] F. Sahli *et al.*, ACS Appl. Energy Mater. **4**, 4333 (2021).
[34] L. Qiu, S. He, Z. Liu, L. K. Ono, D.-Y. Son, Y. Liu, G. Tong, and Y. Qi, J. Mater. Chem. A **8** (2020).
[35] Y. Zhou *et al.*, Adv. Funct. Mater. **31**, 2101058 (2021).
[36] R. Swartwout *et al.*, Solar RRL **6** (2021).
[37] A. Ciccioli and A. Latini, J. Phys. Chem. Lett. **9**, 3756 (2018).
[38] E. J. Juarez-Perez, Z. Hawash, S. R. Raga, L. K. Ono, and Y. Qi, Energy Environ. Sci. **9**, 3406 (2016).
[39] A. Latini, G. Gigli, and A. Ciccioli, Sustain. Energy Fuels **1**, 1351 (2017).
[40] M. Shtein, H. F. Gossenberger, J. B. Benziger, and S. R. Forrest, J. Appl. Phys. **89**, 1470 (2000).
[41] L. Hao, Q. Zhao, X. Wang, S. Pang, and G. Cui, J. Mater. Chem. C **10**, 2390 (2022).
[42] Z. Shao *et al.*, Angew. Chem. **131**, 5643 (2019).
[43] J. Pejnefors, S. L. Zhang, H. H. Radamson, J. V. Grahn, and M. Östling, J. Appl. Phys. **88**, 1655 (2000).
[44] C. V. Thompson, Annu. Rev. Mater. Sci. **30**, 159 (2003).
[45] See supplementary material online for a table of valves and material boats currently on the market, images of material arm, thermocouple readings from the system, and an MAPbI3 XRD graph from the system.

18 September 2024 17:55:02

© Author(s) 2023